Journal of Non-Crystalline Solids 358 (2012) 2626–2634

# Evaluation of the guided random parameterization method for critical cooling rate calculations

Bruno Poletto Rodrigues *,[1], Edgar Dutra Zanotto [1]

*Vitreous Materials Laboratory, Department of Materials Engineering, Federal University of São Carlos, 13565-905, São Carlos, SP, Brazil*

ARTICLE INFO

*Article history:*
Received 10 April 2012
Received in revised form 6 June 2012
Available online 27 June 2012

*Keywords:*
Glass;
Crystallization;
Glass formation;
Critical cooling rate;
Glass forming ability

ABSTRACT

We focus on a recently suggested approach to the calculation of critical cooling rates for glass formation. It is a "random parameterization" method that is guided by a limited number of isothermal scanning calorimetry experiments. However, several assumptions have been made in its derivation that may not mirror the actual crystallization behavior of most supercooled liquids, which may jeopardize the estimation of glass forming ability. We evaluate those assumptions and the applicability of the method is tested for lithium disilicate glass (which displays moderate internal nucleation rates) and dibarium titanium silicate glass (which displays very high internal nucleation rates, similar to those of metallic glasses). Both glasses nucleate homogeneously and exhibit polymorphic crystallization. Our calculations show that some overlooked variables, such as the sample geometry, nucleation induction-times, surface crystallization and the breakdown of the Stokes–Einstein/Eyring equation, have significant roles on the calculated time–temperature–transformation curves during heating experiments. We demonstrate that the proposed random parameterization method can only be used when a glass forming liquid that undergoes internal crystallization is cooled from above its liquidus to various test temperatures. If the sample undergoes predominant surface crystallization or if it is heated to the test temperature several corrections must be made.



## 1. Introduction

Glass science and technology are steadily advancing with the availability of new simulation and experimental techniques, and the discovery of numerous new compositions and forming processes are broadening the application range of glass articles from household items to high technology devices. This flexibility is largely accomplished as a result of unique characteristic properties of the vitreous state and because some properties can only be obtained through the controlled crystallization of glasses leading to modern glass-ceramics. As the demand for new glasses and glass-ceramics increases, knowledge of which compositions vitrify easily and which are reluctant glass formers is of paramount importance and they include fluoride, chalcogenide, salt, metallic and organic glasses in addition to the traditional family of oxide glasses.

This paper focuses on a recent method to calculate the critical cooling rates for glass formation ($R_c$) proposed by Xu et al. [1]. It is theoretically possible to vitrify any material because the kinetic phenomenon of vitrification requires only the avoidance of crystallization during synthesis. Therefore, the speed at which a given liquid must be cooled to vitrify it is of key importance [2]. Hence, the glass forming ability may be described as the minimum cooling rate required to avoid a certain minimum crystallized fraction during quenching of a melt (i.e., the critical cooling rate $R_c$). Good glass forming liquids, such as the ubiquitous window glasses, require quite slow cooling rates ($R_c < 10^{-2}$ K/s), whereas some metallic alloys must be cooled at $> 10^6$ K/s to vitrify [3].

Critical cooling rates can, in principle, be experimentally estimated from the following: i) DSC or DTA cooling curves [4], provided that the equipment is able to melt the specimen and cool it at rates approaching the critical rate; or ii) from the time–temperature–transformation (TTT) or continuous cooling (CCT) curves, which can be extremely time consuming to assemble [5]. There are also ways to theoretically calculate $R_c$ that are derived from qualitative or semi-quantitative analyses using the classical nucleation theory (CNT) and crystal growth models [6–12], but these, especially the CNT, do not have predictive power. Unfortunately, because of several experimental variables, such as sample size, geometry, experimental apparatus, sensitivity and assorted errors, the theoretical and experimental critical cooling rates often diverge.

An interesting recent paper by Xu et al. [1] proposes a new approach to calculate $R_c$ in the absence of thermodynamic and kinetic data. Their method assumes homogeneous steady-state nucleation in the sample interior and utilizes the Johnson–Mehl–Avrami–Komolgorov (JMAK) equation for the minimum volume fraction crystallized ($f_c$) and its relationship with the critical cooling rate:

$$R_c = \left[\frac{4\pi}{3f_c}\left(\int_{T_m}^{T_g} I_{st}(T)\left(\int_{T_m}^{T} u\left(T'\right)dT'\right)^3 dT\right)\right]^{1/4} \quad (1)$$

* Corresponding author.
*E-mail addresses:* bruno.poletto.r@gmail.com (B.P. Rodrigues), dedz@ufscar.br (E.D. Zanotto).
[1] http://lamav.weebly.com/.

0022-3093/$ – see front matter © 2012 Elsevier B.V. All rights reserved.
doi:10.1016/j.jnoncrysol.2012.06.010

where $f_c$ is a (more or less) arbitrary [13,14] upper bound of the crystallized fraction at which a material can still be considered glassy, which is generally assumed to be between $10^{-6}$ and $10^{-2}$; $T_g$ is the laboratory glass transition temperature, which is usually determined by DSC; $T_m$ is the melting point of the crystalline phase for stoichiometric crystallization; $I_{st}$(T) is the steady-state nucleation rate, as given by the classical nucleation theory; $u$(T) is the linear crystal growth rate, as given by the model that best describes the available data. Eq. (1) is valid for isothermal crystallization with simultaneous homogeneous nucleation and growth of spherical crystals in the specimen volume. Other forms of this equation can be used in different situations.

The method proposed in Ref. [1] consists of the following steps: i) measuring the DSC crystallization onset time in isothermal runs at four different temperatures, two below the nose of the TTT curve and two above it; and ii) systematically varying the unknown parameters of the nucleation and crystal growth equations (viscosity, surface tension, thermodynamic driving force, leap distance, and nucleation pre exponential, molar volume), calculating the theoretical value of the crystallization onset time for spherical crystals in the sample interior ($t_{onset}$ — Eq. (2), which is only valid for $f_c$<0.05) for each parameter set and comparing the calculated $t_{onset}$ with the experimental DSC values.

$$t_{onset}(\mathrm{T}) = \left(\frac{3f_c}{\pi I_{st}(\mathrm{T})u(\mathrm{T})^3}\right)^{1/4} \quad (2)$$

Finally, the calculated $R_c$ is validated only if the corresponding parameter set generates calculated crystallization onset times for the four DSC test temperatures that lie close to the experimental values. Xu et al. [1] reported excellent agreement between the value of $R_c$ determined by an independent experimental method (recalescence signal from DSC cooling experiments) and the calculated values from their guided random parameterization (GRP) method for $Zr_{41.2}Ti_{13.8}Cu_{12.5}Ni_{10}Be_{22.5}$ (Vit1) and $Pd_{40}Cu_{30}Ni_{10}P_{20}$ (PNCP) bulk metallic glasses (BMGs).

However, to develop this interesting new method, several assumptions have been made that may not represent the actual crystallization behavior of several materials and may lead to incorrect estimations of $R_c$. These assumptions are discussed below.

First, even if the assumed normal or continuous crystal growth model seems to be applicable to bulk metallic glasses (according to Jackson's criterion [10], it is applicable because of their low entropy of fusion [15,16]), the model assumes short-range structural rearrangement of molecular units from the supercooled liquid to an atomically rough crystal surface that has no preferred bonding sites [17]. This assumption may not hold for bulk metallic glass-forming alloys because they depend upon medium to long range diffusion [18–23], the principle of maximum confusion [22–24] and, consequently, highly non-stoichiometric crystallization [24–29] for vitrification to occur.

Second, in the original formulation provided in Ref. [1], the GRP method can only be applied to glass compositions that nucleate homogeneously and exhibit negligible heterogeneous nucleation (either on the surface or in the sample interior). This requirement poses an additional problem. In fact, the vast majority of glass forming liquids of all classes exhibit predominant heterogeneous nucleation on their external surfaces and defects, and only a small subgroup [30,31] exhibits significant internal homogeneous nucleation in addition to heterogeneous nucleation. This fact is relevant to the present analysis because heterogeneous nucleation can be much faster, or at least be active over a much wider temperature range than homogeneous nucleation [32], implying that crystal growth starting from the sample surface and proceeding towards its interior is normally the main contributor to crystallization. Several variables, such as surface finish, selective oxidation, chemical segregation and surrounding atmosphere have been shown to affect the both the magnitude and kinetics of the surface crystallization of glasses, including BMGs [33–38].

Third, the experimental DSC runs are assumed to be ideally isothermal, neglecting nucleation and growth during the heating or cooling stage necessary to bring the sample from ambient temperature up to the chosen DSC test temperature. Depending on the DSC heating or cooling rate, the test temperature, the intrinsic internal nucleation and growth rates of the material, the magnitude of the nucleation time-lag and the number of active sites on the sample surface ($N_s$), a small to large number of nuclei may form on the surface and sample interior ($N_v$) [39–42] before the sample reaches the DSC test temperature. The heating or cooling stage that passes through the near-$T_g$ temperature range also complicates the use of any classical crystal growth model equations to calculate or fit the $u$(T) data because of the often-reported [3,43–45] breakdown of the Stokes–Einstein/Eyring equation at approximately 1.1–1.2 $T_g$, which generally causes the experimental growth rates to be higher than the theoretical ones.

To test the validity of the GRP method proposed by Xu et al. [1] (in consideration of the potential problems described above), we simulated TTT curves using a plethora of literature data for two stoichiometric crystallizing glasses spanning a wide range of maximum nucleation rates ($I_{max}$): lithium disilicate glass ($Li_2O.2SiO_2$–LS2), which exhibits lower internal homogeneous nucleation rates ($I_{max}$ ~$10^9$ $m^{-3}.s^{-1}$) than most metallic glasses, and dibarium titanium disilicate glass ($2BaO.TiO_2.2SiO_2$ — B2TS2 = fresnoite), which exhibits internal homogeneous nucleation rates ($I_{max}$~$10^{17}$ $m^{-3}.s^{-1}$) that are comparable to those reported for metallic-glass-forming systems.

## 2. Materials and calculation procedures

In this study, we used the following simulated DSC run: heating from ambient temperature to the chosen isothermal test temperature at the maximum possible heating rate (for instance, 40 K/min in our Neztsch DSC404) and holding at that temperature until the beginning of crystallization, assumed to be 1% vol. (other values such as 0.1% and 5% were tested and did not affect our conclusions). In this way, $t_{onset}$ was calculated for several temperatures from $T_g$ to $T_m$.

The TTT curves were calculated using data available in the literature. The steady-state homogeneous nucleation rates can be described by the CNT, according to Eq. (3). For LS2 glass [46] and B2TS2 glass [17], the screw dislocation model (Eq. (4)) provides a good description of the crystal growth rates in the high temperature range for which the Stokes–Einstein/Eyring relation is valid. Below a certain breakdown temperature ($T_b$ ~1.15$T_g$) [3,43–45], the crystal growth rates are well described by an Arrhenius law (Eq. (5)) [45,46].

$$I_{st}(\mathrm{T}) = \frac{\mathrm{A}\cdot\mathrm{T}}{\eta(\mathrm{T})}\exp\left(-\frac{16\cdot^3\cdot V_m{}^2}{3k\cdot T\cdot \Delta G(T)^2}\right) \quad (3)$$

$$u_{sd}(\mathrm{T}) = \frac{k\cdot|\Delta G(\mathrm{T})|\cdot\mathrm{T}}{4\pi\cdot\lambda\cdot\sigma\cdot\eta(T)}\left[1-\exp\left(-\frac{|\Delta G(\mathrm{T})|}{R\cdot\mathrm{T}}\right)\right] \quad (4)$$

$$u_b(\mathrm{T}) = u_0\exp\left(-\frac{Q_u}{R\cdot\mathrm{T}}\right) \quad (5)$$

where $A$ is the (fitted) CNT pre-exponential, σ the (fitted) nucleus/glass surface energy, $V_m$ is the crystal molar volume, $k$ is the Boltzmann constant, $R$ is the ideal gas constant, λ is the leap distance (usually of the same order of magnitude as the crystal lattice parameter [17]), $u_0$ is the Arrhenian growth pre exponential, $Q_u$ is the Arrhenian growth activation energy; $\eta$(T) is the experimental viscosity, which was modeled with the Vogel–Fulcher–Tamman equation (Eq. (6)); and $\Delta G$(T) is the thermodynamic driving force, which was modeled by the Turnbull approximation (Eq. (7)). This approximation gives good estimates for LS2 [42] and B2TS2.

$$\log(\eta(\mathrm{T})) = \log(\eta_\infty) + \frac{B}{T-T_0} \quad (6)$$

$$\Delta G(\mathrm{T}) = \Delta H_{\mathrm{m}}(1-\mathrm{T}/\mathrm{T_m}) \tag{7}$$

While the Vogel–Fulcher–Tamman equation is a classical model used in Ref. [1], a new and more accurate equation has been proposed by Mauro et al. [48]. We performed our calculations with both equations and found very little difference. Even though these equations diverge strongly for temperatures below $T_g$ and above $T_m$, we are concerned with processes occurring in the interval between $T_g$ and $T_m$, where the calculated viscosities from both models are quite similar.

The crystallization of both glasses studied occurs through the growth of ellipsoidal crystals [40,47]; therefore, to estimate the crystallized volume fraction, the crystal growth rates for the smaller axes and larger axis should be known. However, data from the available literature usually concern only the largest axis, therefore using this crystal growth rate overestimates the crystallized fraction at any given time. To achieve more reliable estimates, we made the reasonable assumption (corroborated by the observed crystal morphology) that the crystal growth rate of the larger axis is twice the rate of the smaller axes ($u_{max}=2u_{min}$), leading to an "effective" crystal growth rate, which is given by (Eq. (8)). This correction is valid when the crystal morphology is ellipsoidal; therefore, in the expressions regarding the growth of uniform layers (Eqs. (21) and (22)), the fastest growth rate is assumed.

$$u_{eff}(\mathrm{T}) = \sqrt[3]{u_{min}(\mathrm{T})^2 \cdot u_{max}(\mathrm{T})} = \frac{u_{max}(\mathrm{T})}{\sqrt[3]{4}} \tag{8}$$

In addition, because our calculations refer to non-isothermal conditions (heating to the DSC test temperature), it is also necessary to correct the crystal nucleation rates by the temperature-dependent nucleation time-lags $\tau(\mathrm{T})$ (Eq. (9) [42]). To apply this correction, we used an approximation derived and tested by Gutzow [49] (Eq. (10)) for the Collins–Kashchiev equation:

$$t(\mathrm{T}) = t_0 \exp\left(\frac{Q_\tau}{R\cdot \mathrm{T}}\right) \tag{9}$$

$$I(t,\mathrm{T}) = I_{st}(\mathrm{T}) \exp\left(-\frac{t(\mathrm{T})}{t}\right) \tag{10}$$

where $\tau_0$ is the nucleation time-lag pre-exponential; $Q_\tau$ is the nucleation time-lag activation energy; and $t$ is the time.

Two sample geometries were considered in our calculations: a 2 mm × 2 mm × 100 μm thin plate and a 3 mm × 3 mm × 3 mm cube, which represent the approximate maximum sample size that fits in a typical DSC pan.

From the published crystal nucleation rate, nucleation time lag, crystal growth rate and sample geometry data, we calculated the crystallization onset times (assuming a crystallized volume fraction of 1%; $\alpha = 1\%$) for three different scenarios:

i) Isothermal simultaneous steady-state homogeneous nucleation and growth of spherical crystals (i.e., no nucleation and growth in the heating or cooling path to the desired treatment temperature), as originally proposed in Ref. [1]:

$$\alpha(t,\mathrm{T}) = 1-\exp\left(-\frac{\pi\cdot I_{st}(\mathrm{T})\cdot u_{eff}(\mathrm{T})^3\cdot t^4}{3}\right) \tag{11}$$

ii) Growth of the internal nuclei formed during heating from room temperature to the test temperature, plus further homogeneous nucleation and growth at the test temperature, with negligible surface crystallization ($N_s = 0$):

$$\alpha(t,\mathrm{T}) = 1-\exp\left[\left(-\frac{\pi\cdot I(\mathrm{T})\cdot u_{eff}(\mathrm{T})^3\cdot t^4}{3}\right)+\left(-\frac{4\pi\cdot N_v(\mathrm{q},\mathrm{T})\cdot u_{eff}(\mathrm{T})^3\cdot t^3}{3}\right)\right] \tag{12}$$

where $N_v(\mathrm{q,T})$ (Eq. (13)) is the density of critical nuclei per unit volume that cumulatively form during heating from below $T_g$ to the DSC test temperature T at a heating rate q.

$$N_v(q,\mathrm{T}) = \int_{T_g-30}^{T} \frac{I\left(\mathrm{T}'\right)}{\mathrm{q}}\, dT' \tag{13}$$

And $I(\mathrm{T})$ should be corrected by the nucleation time lags. Considering a constant heating rate $q = \mathrm{T}/t$, Eq. (8) becomes $q$-dependent (Eq. (14)):

$$I(q,\mathrm{T}) = I_{st}(\mathrm{T})\exp\left(-\frac{t(\mathrm{T})\cdot q}{\mathrm{T}}\right) \tag{14}$$

Therefore, Eq. (13) becomes the following:

$$N_v(q,\mathrm{T}) = \int_{T_g-30}^{T} \frac{I_{st}\left(\mathrm{T}'\right)\exp\left(-\frac{t\left(\mathrm{T}'\right)\cdot q}{\mathrm{T}'}\right)}{q}\, dT' \tag{15}$$

Eqs. (12) and (15) rely on two intrinsic assumptions: first, the critical nuclei that form at lower temperatures grow enough on the heating path that they do not dissolve back into the parent glass at higher temperatures; second, during the heating stage the cumulative crystallized fraction remains negligible, meaning that all nucleated crystals are only slightly larger than their critical size at the test temperature.

Nuclei dissolution can be tested by comparing the nucleus critical size (R*) as a function of temperature (Eq. (16), as given in Ref. [42]) and the crystal radius (r) as a function of temperature and heating rate (Eq. (17)).

$$\mathrm{R}^*(\mathrm{T}) = \frac{2\cdot\sigma\cdot V_m}{\Delta G(\mathrm{T})} \tag{16}$$

$$\mathrm{r}(q,\mathrm{T}) = \mathrm{R}^*(\mathrm{T}) + \int_{T_g-30}^{T} \frac{u\left(\mathrm{T}'\right)}{q}\, dT' \tag{17}$$

Figs. 1 and 2 illustrate the calculated R* and r for LS2 glass and B2TS2 glass, respectively. They show that no dissolution should occur for nuclei formed at $T_g$ with the heating rate used in our calculations (40 K/min).

However, there is a temperature range for which nuclei dissolution could occur for LS2; for instance between $T_g$ and 752 K at very high heating rates ($q = 400$ K/min). But heating rates of this magnitude are not normally used in DSC experiments and are only shown here to illustrate the phenomenon.

The cumulative crystallized fraction during heating ($\alpha_{heat}$) was calculated by rewriting Eq. (1) as shown below, but this procedure poses a problem. As we mentioned previously, the decoupling of the viscosity and transport parts of the crystal growth at $T_b$ [3,43–45] divides the growth data into two sets: one set below $T_b$, which is described by an Arrhenian equation (Eq. (5)), and one above $T_b$, which is well described by the screw dislocation crystal growth model using the viscosity (Eq. (4)) for both glasses. Therefore, it is necessary to consider this change in crystal growth behavior at $T_b$. This consideration is shown in Eq. (18)

$$\begin{aligned}\alpha_{\mathrm{heat}}(q,\mathrm{T}) = 1-\exp([-\Phi(\mathrm{T_b}-\mathrm{T})\cdot X_b(q,\mathrm{T})]\\ +[-\Phi(\mathrm{T}-\mathrm{T_b})\cdot(X_b(q,\mathrm{T_b})+X_{sd}(q,\mathrm{T}))])\end{aligned} \tag{18}$$

where $\Phi(\mathrm{T})$ is the Heaviside step function, $T_b$ is the breakdown

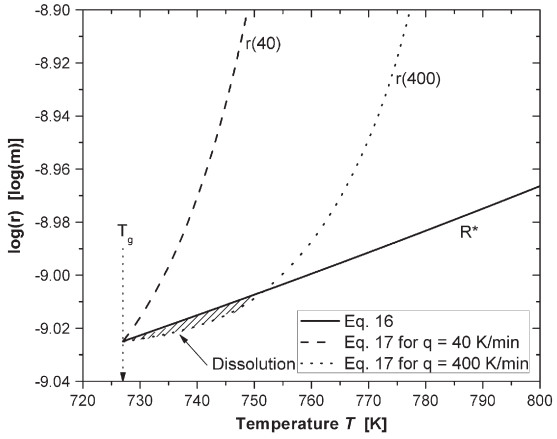


**Fig. 1.** Critical nucleus radius (R* — Eq. (16)) and crystal radius (r — Eq. (17)) for LS2 glass.

temperature and $X_b$ and $X_{sd}$ are given by Eqs. (19) and (20), respectively.

$$X_b(q,\mathrm{T}) = \frac{4\pi}{3q^4}\left[\int_{\mathrm{T_g}-30}^{\mathrm{T}} I\left(q,\mathrm{T}'\right)\left(\int_{\mathrm{T_g}-30}^{\mathrm{T}'} \frac{u_b\left(\mathrm{T}''\right)}{\sqrt[3]{4}dT''}\right)^3 dT'\right] \quad (19)$$

$$X_{sd}(q,\mathrm{T}) = \frac{4\pi}{3q^4}\left[\int_{\mathrm{T_b}}^{\mathrm{T}} I\left(q,\mathrm{T}'\right)\left(\int_{\mathrm{T_b}}^{\mathrm{T}'} \frac{u_{sd}\left(\mathrm{T}''\right)}{\sqrt[3]{4}dT''}\right)^3 dT'\right] \quad (20)$$

with the nucleation rates corrected for non steady-state effects by the Gutzow approximation (Eq. (14)).

Eq. (18) yields maximum values of crystallized fraction during heating $\alpha_{heat}(40,T_m) = 2\cdot10^{-15}$ for LS2 glass and $\alpha_{heat}(40,T_m) = 7\cdot10^{-6}$ for B2TS2 glass. Therefore, the assumptions required for applying Eq. (12) to the entire temperature range from $T_g$ to $T_m$ seem reasonable.

iii) The third scenario is the following: negligible $N_v$ is formed on the heating path, but $N_s$ is large enough to form a uniform crystallized surface layer that grows toward the specimen interior for thin plate (Eq. (21)) and cubic (Eq. (22)) specimens:

$$\alpha(t,\mathrm{T}) = \frac{2\cdot u(\mathrm{T})\cdot t}{e} \quad (21)$$

$$\alpha(t,\mathrm{T}) = \frac{L^3-(L-2\cdot u(\mathrm{T})\cdot t)^3}{L^3} \quad (22)$$

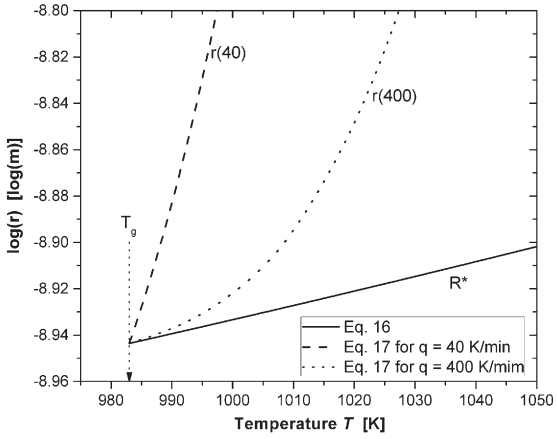


**Fig. 2.** Critical nucleus radius (R* — Eq. (16)) and crystal radius (r — Eq. (17)) for B2TS2 glass.

where $e$ is the specimen thickness and $L$ is the cube side. Note that Eqs. (21) and (22) are only valid for $2\cdot u(\mathrm{T})\cdot t/e \le 1$ and $2\cdot u(\mathrm{T})\cdot t/L \le 1$, respectively.

## 3. Results

### 3.1. Lithium disilicate glass

The viscosity, kinetic and thermodynamic data for LS2 were taken from Nascimento [17]. Figs. 3 and 4 show the experimental crystal nucleation and growth rates fitted with the classical models. These fits produced the following values: nucleation pre-exponential $A = 10^{49.81}$ Pa.m$^{-3}$.s$^{-2}$.K$^{-1}$, surface energy $\sigma = 0.195$ J.m$^{-2}$ for the CNT (Eq. (3)). Regarding crystal growth rates, the following values were obtained: $\lambda = 0.19$ Å for the screw dislocation growth model (Eq. (4)) and $u_0 = 6.55\cdot10^{12}$ m.s$^{-1}$ and $Q_u = 337507$ J.mol$^{-1}$ below the breakdown (Eq. (5)). With these data the crystallization onset times for LS2 glass were calculated for four different crystallization scenarios on the heating path (Fig. 5).

### 3.2. Dibarium titanium disilicate glass

The viscosity, kinetic and thermodynamic data for B2TS2 were taken from Refs. [17,47,62]. Figs. 6 and 7 show literature data [47,63] for crystal nucleation and growth rates fitted with classical models. These fits produced the following values: nucleation pre-exponential $A = 10^{64.73}$ Pa.m$^{-3}$.s$^{-2}$.K$^{-1}$ and surface energy $\sigma = 0.225$ J.m$^{-2}$ for the CNT (Eq. (3)), $\lambda = 9.1$ Å for the screw dislocation growth model (Eq. (4)) and $u_0 = 8.17\cdot10^{15}$ m.s$^{-1}$ and $Q_u = 505111$ J.mol$^{-1}$ below the breakdown (Eq. (5)). With these data the crystallization onset times for B2TS2 glass were calculated for four different crystallization scenarios on the heating path (Fig. 8).

## 4. Discussion

The calculated crystallization onset times from the heating experiments shown in Figs. 5 and 8 demonstrate that the "pure" JMAK regime (Eq. (11)) (i.e., homogeneous internal nucleation and simultaneous growth), which was suggested in Ref. [1] to control the overall crystallization kinetics in the entire $T_g$ to $T_m$ range, differs significantly from the other two possible scenarios. These simulations clearly show that the isothermal JMAK kinetics only describes the process around $T_g$ in cubic samples and systems with high enough internal nucleation rates, such as the dibarium titanium disilicate (and possibly some metallic glasses). In the following sessions, we show that several

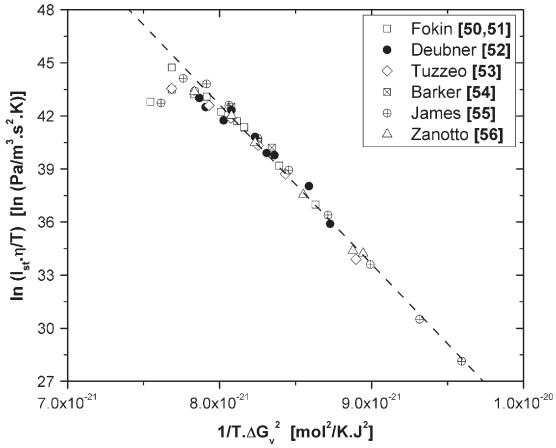


**Fig. 3.** Crystal nucleation rates from Refs. [50–56] and CNT fit for LS2. The resulting values are: $A = 10^{49.81}$ Pa.m$^{-3}$.s$^{-2}$.K$^{-1}$ and $\sigma = 0.195$ J.m$^{-2}$ (squared Pearson coefficient $r^2 = 0.993$ and standard error of regression (SER) of $10^{0.91}$ Pa.m$^{-3}$.s$^{-2}$.K$^{-1}$ and 0.059 J.m$^{-2}$, respectively).

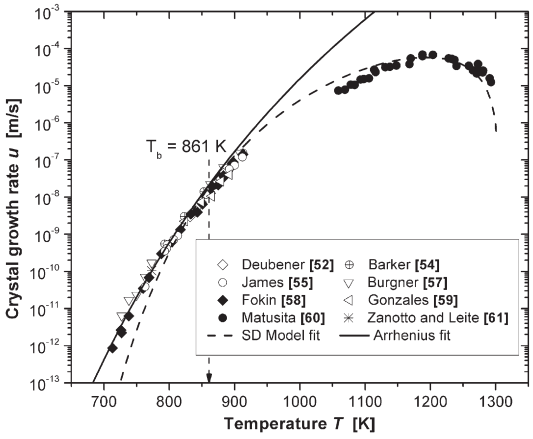


**Fig. 4.** Crystal growth rate data from Refs. [52,54,55,57–61] in addition to the fitted Arrhenius equation and screw dislocation growth model. $\lambda = 19 \cdot 10^{-2}$ Å ($r^2 = 0.934$ and SER of $0.72 \cdot 10^{-2}$ Å) for the screw dislocation growth, $u_0 = 6.55 \cdot 10^{12}$ m.s$^{-1}$ and $Q_u = 337507$ J.mol$^{-1}$ ($r^2 = 0.980$ and SER of 5.27 m.s$^{-1}$ and 10624 J.mol$^{-1}$, respectively) below the breakdown temperature.

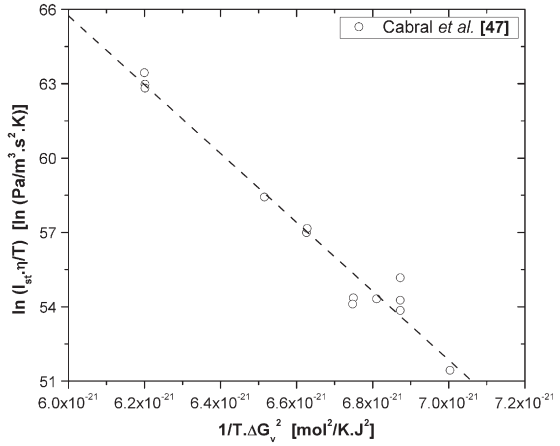


**Fig. 6.** Crystal nucleation rates and CNT fit of data for B2TS2 [47]. The resulting values were $A = 10^{64.73}$ Pa.m$^{-3}$.s$^{-2}$.K$^{-1}$ and $\sigma = 0.225$ J.m$^{-2}$ ($r^2 = 0.966$ and SER of $10^{2.17}$ Pa.m$^{-3}$.s$^{-2}$.K$^{-1}$ and 0.085 J.m$^{-2}$, respectively).

previously overlooked variables explain the mismatch between the pure JMAK regime (isothermal simultaneous internal nucleation and growth) and the two other simulated crystallization scenarios.

### 4.1. Influence of the nuclei formed during heating

In the method proposed in Ref. [1], it is assumed that the DSC runs are ideally isothermal. However, these runs must be made in real DSC equipment that requires a heating stage to bring the sample from ambient temperature up to the DSC test temperature. Because the test temperatures must be higher than $T_g$ and the internal homogeneous nucleation rate often reaches its maximum near $T_g$ (depending on the system's intrinsic nucleation rate), a certain number of nuclei may form during heating. Fig. 9 illustrates this effect for the LS2 glass: in the region near $T_g$, the heating stage is quite short; therefore, few crystals are formed and isothermal crystallization at the test temperature dominates. However, as the temperature rises, two factors begin to change this balance. First, the number of nuclei formed during the heating stage increases as the time to reach higher temperature becomes longer. Then, the number of nuclei becomes nearly constant at approximately 800 K because the nucleation rate above this temperature is negligible. Second, as the crystal growth rate increases with temperature and the nucleated crystals do not dissolve back into the parent glass at least not for the typical 40 K/min heating rate considered here, as shown in Figs. 1 and 2, the crystallization onset times during the heating stage follow the crystal growth rate curve.

Therefore, near and just above $T_g$, the nuclei formed during the heating stage through $T_g$ do change the overall crystallization kinetics of the glass from those of simultaneous homogeneous nucleation and growth. However, at high temperatures, only the growth of the nuclei formed during the heating path occurs.

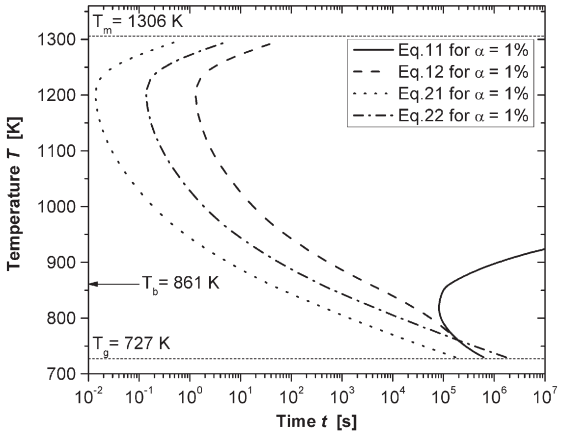


**Fig. 5.** Calculated TTT curves for a LS2 sample on the heating path for four possible scenarios. Eq. (11) = isothermal simultaneous homogeneous (internal) nucleation and growth of spherical crystals (JMAK) at each temperature. Eq. (12) = growth of the internal nuclei formed on the heating path from room temperature to a test temperature T, in addition to additional homogeneous nucleation and growth at the test temperature (JMAK). Eq. (21) = growth of a uniform crystalline layer from the surface to the sample interior in a thin plate with negligible $N_v$. Eq. (22) = growth of a uniform crystalline layer from the surface to the sample interior in a cube with negligible $N_v$.

### 4.2. Influence of the breakdown of the Stokes–Einstein/Eyring equation

Figs. 4 and 7 show that the best crystal growth model only describes the crystal growth rate data from a certain breakdown temperature ($T_b$) up to the melting point. Below $T_b$, the viscosity controlled diffusivity is decoupled from the effective diffusivity for crystal growth, which leads to an underestimation of the crystal growth rates calculated by the available growth models that use the viscosity as the transport controller. Below $T_b$, the actual crystal growth rates can be orders of magnitude faster than the predicted values calculated assuming the validity of the Stokes–Einstein equation. This difference leads to underestimated onset times in the TTT

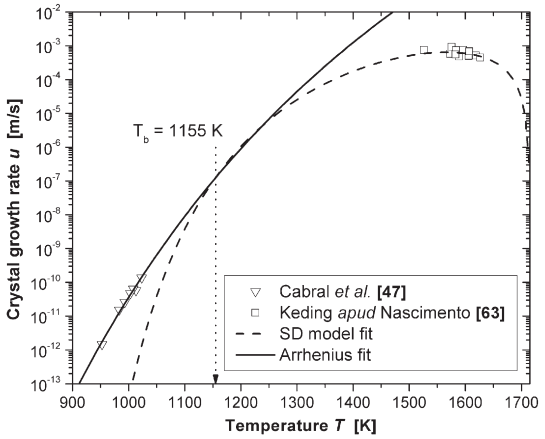


**Fig. 7.** Crystal growth data from Refs. [47,63] and fitted Arrhenius equation and screw dislocation growth model. $\lambda = 9.10$ Å ($r^2 = 0.221$ and SER of 0.55 Å) for the screw dislocation growth, $u_0 = 8.17 \cdot 10^{15}$ m.s$^{-1}$ and $Q_u = 505111$ J.mol$^{-1}$ ($r^2 = 0.984$ and SER of 25.18 m.s$^{-1}$ and 26712 J.mol$^{-1}$, respectively) below the breakdown.

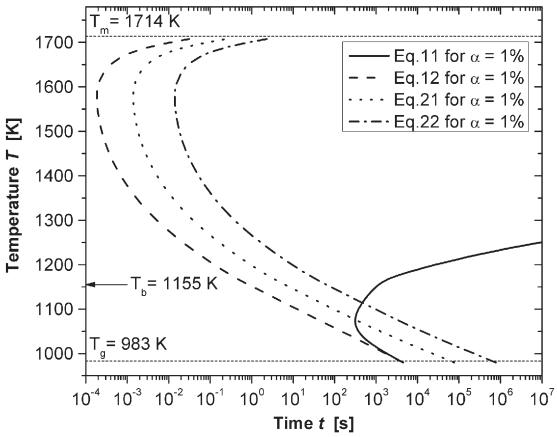


**Fig. 8.** Calculated TTT curves for a B2TS2 sample on the heating path for four possible scenarios. Eq. (11) = isothermal simultaneous homogeneous (internal) nucleation and growth of spherical crystals (JMAK) at each temperature. Eq. (12) = growth of the internal nuclei formed on the heating path from room temperature to a test temperature T, in addition to additional homogeneous nucleation and growth at the test temperature (JMAK). Eq. (21) = growth of a uniform crystalline layer from the surface to the sample interior in a thin plate with negligible $N_v$. Eq. (22) = growth of a uniform crystalline layer from the surface to the sample interior in a cube with negligible $N_v$.

curves (calculated without considering the breakdown), as observed in Figs. 10 and 11 for LS2 glass and B2TS2 glass, respectively. Further evidence of the importance of this effect is provided by the experimental crystallization data from Refs. [47,61], which are plotted along with the simulated curves. These results are much more consistent when the breakdown is considered.

The underestimation of the calculated crystal growth rates becomes larger as the treatment temperature approaches $T_g$. This underestimation can be approximately one order of magnitude for the LS2 glass and up to three orders of magnitude for the B2TS2 glass. This difference could be caused by a poor fit of the crystal growth model and lack of crystal growth rate data for the B2TS2 glass, but in the thoroughly studied LS2 system, this discrepancy is not negligible. Therefore, the breakdown of the SE/E equation is a variable that must be included when considering the overall crystallization kinetics in the neighborhood of $T_g$.

Here, it should be stressed that although our calculations only use an estimate (Eq. (8)) concerning the ellipsoidal shape of the crystals that develop in both glasses [42,61], the fair coincidence between

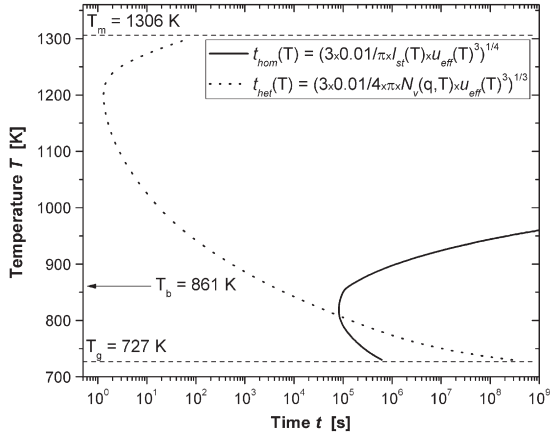


**Fig. 9.** Comparison of crystallization onset times during heating of LS2 glass, considering 1% crystallized fraction: i) $t_{hom}$ = isothermal homogeneous nucleation and growth at any temperature T (Eq. (11)) and; ii) $t_{het}$ = homogeneous nucleation on the heating path plus pure growth of the internal crystals formed during heating, as given by Eq. (15) with $q = 40$ K/min.

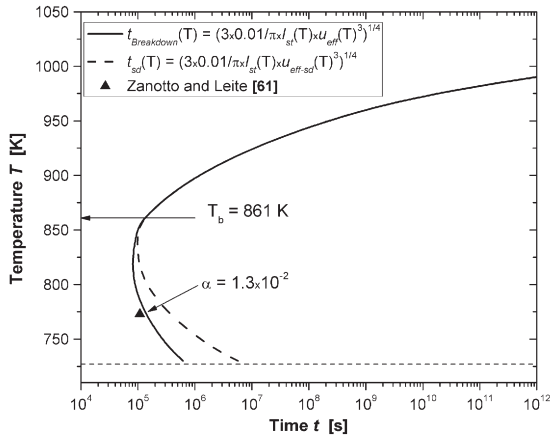


**Fig. 10.** Simulated TTT curves for LS2 glass ($f_c = 1\%$, according to Eq. (2)) using the screw dislocation growth model above and below $T_b$ ($t_{sd}$ — dashed line) and using the Arrhenius equation below $T_b$ ($t_{Breakdown}$ — solid line). The experimental data point at 773 K is from Ref. [61].

the calculated curves and the experimental data for the LS2 and B2TS2 glasses corroborates the consistency of our assumptions and simulations.

### 4.3. Influence of sample geometry

When one considers that a pure JMAK regime (as given by Eq. (1) in Ref. [1], describing isothermal steady-state simultaneous homogeneous internal nucleation and growth) controls the overall crystallization kinetics, the sample geometry plays no effective role. However, if the sample also crystallizes from its surface to its interior, as is usually observed in practice, the sample size and shape become important variables. These geometric inputs, together with the material's intrinsic nucleation rate, determine the mechanism that dominates the overall crystallization kinetics. In the case of a thin sample of LS2 (Eq. (21) in Fig. 5), a glass with moderate internal nucleation rates ($I_{max} \sim 10^9\ m^{-3}.s^{-1}$), the surface dominates the overall crystallization for almost the entire range from $T_g$ to $T_m$, except near $T_g$, where the nucleation rates are highest and the crystal growth rates are slow; then, a pure JMAK regime controls the crystallization. In a cubic sample, although the surface begins to crystallize sooner, it is the growth of the nuclei formed in the sample volume during heating that controls the overall crystallization, as shown in Fig. 12.

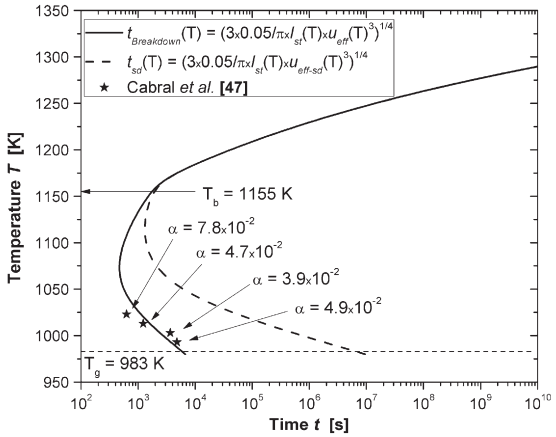


**Fig. 11.** Simulated TTT curves for B2TS2 glass ($f_c = 5\%$, according to Eq. (2)), in which the screw dislocation growth model is applied above and below $T_b$ ($t_{sd}$ — dashed line) and the Arrhenius equation is used below $T_b$ ($t_{Breakdown}$ — solid line). Experimental data points at 993, 1003, 1013 and 1023 K are from Ref. [47].

Considering a cubic sample (Eq. (22) in Fig. 5), which has a smaller surface area to volume ratio ($2 \cdot 10^3$ m$^{-1}$ compared to $22 \cdot 10^3$ m$^{-1}$ for the thin plate), the JMAK regime and the growth of pre-existing crystals nucleated on the heating path dominate the overall crystallization kinetics over the entire temperature range. For B2TS2 glass, which exhibits the highest internal nucleation rates ever reported [47,62] for oxide glasses ($I_{max} \sim 10^{17}$ m$^{-3}$.s$^{-1}$), the overall crystallization mechanism is effectively geometry independent (Figs. 8 and 13) because homogeneous nucleation during heating overrides the surface crystallization.

### 4.4. Influence of the nucleation time-lag

Because the simulated DSC runs have a heating step, the fact that the nucleation rate does not reach its steady-state instantaneously at each temperature must be considered. The nucleation induction time is composition- and temperature-dependent, and it causes a non-negligible shift of the calculated TTT curves, as shown in Fig. 14. In that figure, the ratio between the crystallization onset times calculated without and with the nucleation time lags is plotted against the reduced temperature ($T_r = T/T_m$) for both glasses. Higher temperatures produce greater effects because the (non-isothermal) heating stage is active for a longer period. When the nucleation time lags are considered, the maximum predicted onset times are approximately 2.3 times slower for LS2 glass and approximately 1.2 times slower for B2TS2 glass.

In light of the above discussion of the possible difficulties of the GRP method, we were initially surprised by the reported agreement between the calculations by GRP and the experimental values of the critical cooling rates for Vit1 and PCNP in Ref. [1]. However, after a closer analysis of the means by which the calorimetric data were acquired [3,64], the reason for the agreement becomes clear. In contrast to our initial understanding, which involved heating a sample through its $T_g$ to the isothermal DSC test temperatures, the onset times used by Xu et al. [1] were obtained by melting a sample and then cooling it to the test temperature. This procedure may significantly change the calculation of the number of crystals that form in a specimen during its trajectory to the isothermal test temperature, which is given by Eq. (15) for heating. This expression should be modified for cooling, leading to Eq. (23):

$$N_{v,cool}(q,T) = \int_{T_m}^{T} \frac{I_{st}\left(T'\right)\exp\left(-\frac{t(T')\cdot -|q|}{T'}\right)}{-|q|} dT' \qquad (23)$$

Fig. 15 shows that these two different paths (heating and cooling) to the isothermal test temperature change the shape of the TTT curve

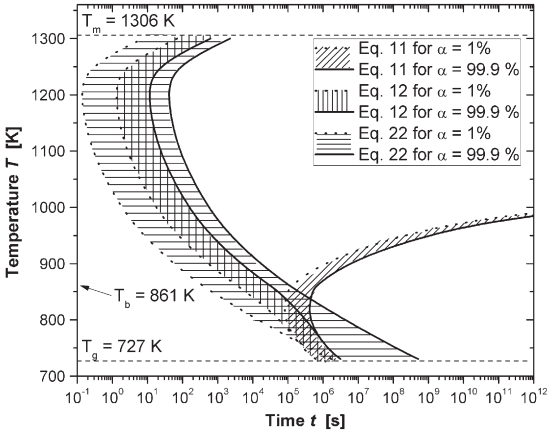


**Fig. 12.** Calculated TTT curves from α = 1% to 99.9% during heating of an LS2 cubic sample.

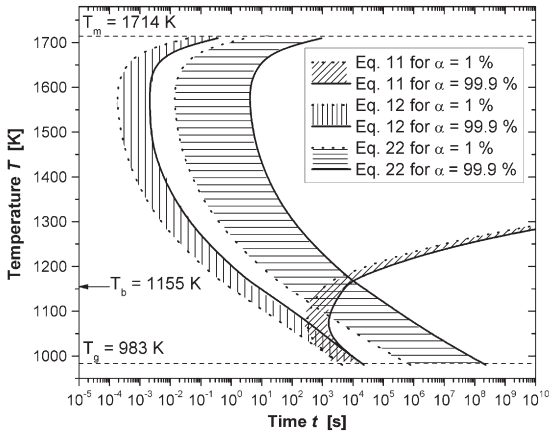


**Fig. 13.** Calculated TTT curves from α = 1% to 99.9% during heating of a B2TS2 cubic sample.

for the B2TS2 glass (which most closely mirrors the behavior of the metallic glasses analyzed in Refs. [3,64]).

As we demonstrated above, the degree of crystallization during the heating of a sample from ambient temperature to a DSC test temperature only coincides with the case of isothermal crystallization near the glass transition temperature. For higher temperatures, the two crystallization onset times diverge significantly. When a sample that displays significant internal nucleation is cooled from the true liquid state above $T_m$ to several DSC test temperatures, agreement with the predicted isothermal JMAK onset times is observed for nearly the entire temperature range. The experimental and simulated onset times differ only for temperatures close to $T_g$, but the difference is less than one order of magnitude for the B2TS2 glass (and inferentially for most metallic glasses). However, if the studied glass-forming liquid undergoes predominant surface nucleation, as shown in Fig. 16, the same restrictions discussed for heating experiments apply to cooling experiments; in other words, the current GRP method cannot be used.

The isothermal JMAK crystallization onset times neglect nucleation and growth on the heating and cooling paths; but these times are equal, whether the samples are heated from ambient temperature or cooled from the melt. However, Figs. 5 and 8 cannot be used for comparison with cooling experiments unless the sample geometry is maintained after melting and the density of surface nucleation sites is infinite. These considerations do not hold in real experiments, as Refs. [3,64] show. In these studies, graphite crucibles were used to

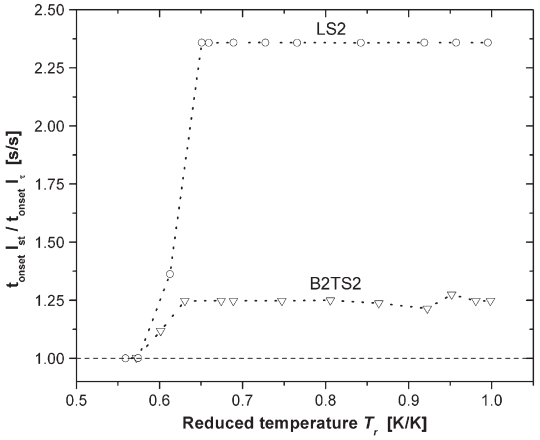


**Fig. 14.** Ratio between the onset times from steady-state nucleation rate and time-lag dependent nucleation rate versus reduced temperature ($T_r = T/T_m$). The crystallization onset times on heating were calculated by Eq. (12) for α = 1% for LS2 and B2TS2 glasses.

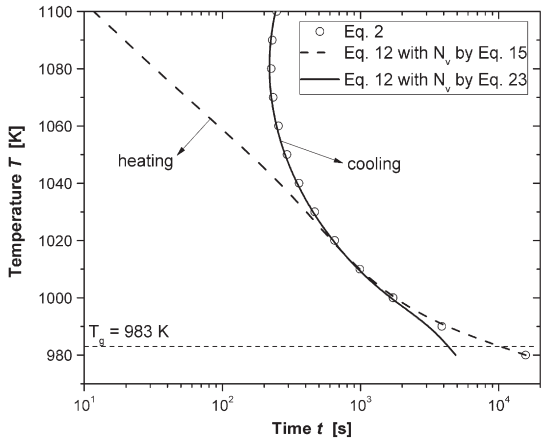


**Fig. 15.** Crystallization onset times for B2TS2 glass ($\alpha = 1\%$). A comparison between pure isothermal crystallization, as given by Eq. (2) (assuming that nothing happens during the heating or cooling path to the desired crystallization temperature), and crystallization considering the effect of nucleation and growth on the path to the isothermal condition (Eq. (12)) by either heating from ambient temperature ($N_v$ given by Eq. (15)) or cooling from the melt ($N_v$ given by Eq. (23)), with $q = 40$ K/min for both cases.

hold the samples during the DSC runs, which have two effects that favor internal crystallization as a result of graphite's extremely low wettability to metallic liquids [65]. First, as the sample is first melted above its liquidus and the wetting angle is high, it tends to spheroidize, minimizing its surface area to volume ratio; second, as the sample becomes spherical, its surface in contact with the crucible walls is greatly reduced, which presumably also reduces the density of the surface nucleation sites. These comments are only valid for special DSC pans (e.g., graphite or vitreous carbon). For typical Pt and alumina pans, all molten oxide liquids significantly wet the pan walls, creating a plethora of surface nucleation sites. In this last case, the current GRP method should not work.

## 5. Summary and conclusions

The guided random parameterization (GRP) method proposed in Ref. [1] for the calculation of the critical cooling rates for vitrification was critically examined and tested with two silicate glass-forming systems, lithium disilicate and dibarium titanium disilicate, which span a wide range of internal nucleation rates. Using data available in the literature, the crystal nucleation and crystal growth rates were modeled taking into account the breakdown of the Stokes–Einstein/Eyring equation at deep undercoolings. TTT curves were calculated for different crystallization scenarios: isothermal internal nucleation and growth, growth of nuclei formed during heating plus isothermal internal nucleation and growth, and surface crystallization on heating.

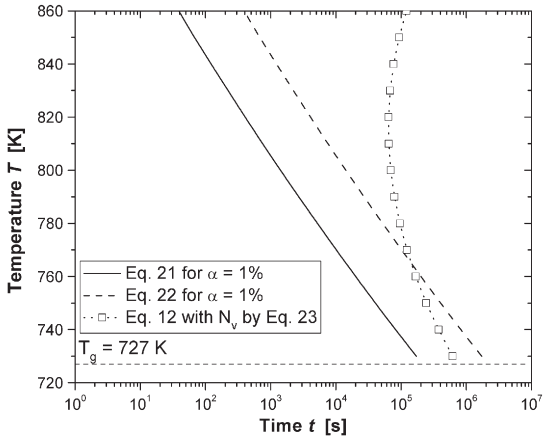


**Fig. 16.** The squares show the calculated crystallization onset times (calculated from Eq. (12), $N_v$ given by Eq. (23), $q = 40$ K/min and $\alpha = 1\%$) for homogeneous nucleation during cooling. The solid and dashed lines refer to pure surface crystallization for thin plates (Eq. (21)) and cubes (Eq. (22)), respectively.

We found that some variables that are not considered in the original GRP method, such as the nuclei formed on the heating path, the sample geometry, surface crystallization and the breakdown of the Stokes-Einstein/Eyring equation, significantly impact the overall crystallization kinetics and the resulting critical cooling rates. For both silicate systems, the isothermal JMAK equation does not describe the overall crystallization kinetics if the sample is heated from ambient temperature to the DSC test temperature; consequently, the present GRP method cannot be used. However, if a liquid is cooled from the melt to a DSC test temperature and internal nucleation predominates over surface nucleation, the experimental and calculated isothermal onset times should be similar, and the method can thus be successfully applied. But for glasses undergoing predominant surface nucleation, this method cannot be used.

## List of symbols and acronyms

| | |
|---|---|
| $\alpha$ | crystallized volume fraction |
| $\Delta G$ | thermodynamic driving force |
| $\Phi(x)$ | heaviside step function |
| $\eta$ | viscosity |
| $\lambda$ | leap distance |
| $\sigma$ | nucleus/glass surface energy |
| $\tau(T)$ | nucleation time-lag |
| $\tau 0$ | nucleation time-lag pre-exponential term |
| A | classical nucleation theory pre-exponential term |
| B2TS2 | dibarium titanium disilicate glass, also known as fresnoite glass |
| BMG | bulk metallic glass |
| CNT | classical nucleation theory |
| DSC | differential scanning calorimetry |
| e | thin plate thickness |
| $f_c$ | upper bound of crystallized fraction at which the material can still be considered glassy |
| GRP | guided random parameterization |
| $I(T)$ | crystal nucleation rate |
| $I_{max}$ | maximum crystal nucleation rate of homogeneous nucleation |
| $I_{st}(T)$ | steady-state crystal nucleation rate |
| JMAK | Johnson–Mehl–Avrami–Komolgorov |
| k | Boltzmann constant |
| L | cube side |
| LS2 | lithium disilicate glass |
| $N_s$ | surface density of crystals |
| $N_v$ | volume density of crystals |
| PCNP | bulk metallic glass of composition $Pd_{40}Cu_{30}Ni_{10}P_{20}$ |
| q | heating rate |
| $Q_\tau$ | nucleation time-lag activation energy |
| $Q_u$ | Arrhenian crystal growth activation energy |
| r | crystal radius |
| $r^2$ | squared Pearson coefficient |
| R | ideal gas constant |
| $R^*$ | nucleus critical size |
| $R_c$ | critical cooling rate for glass formation |
| SE/E | Stokes–Einstein/Eyring |
| SER | standard error of regression |
| t | time |
| $t_{onset}$ | onset time for crystallization |
| $T_b$ | Stokes–Einstein/Eyring equation breakdown temperature |
| $T_g$ | glass transition temperature |
| $T_m$ | melting point of the crystalline phase |
| TTT | time–temperature–transformation |

| | |
|---|---|
| $u(T)$ | crystal growth rate |
| $u_0$ | Arrhenian crystal growth pre-exponential term |
| $u_{max}$ | maximum crystal growth rate measured in a given direction |
| $u_{min}$ | minimum crystal growth rate measured in a given direction |
| $u_{eff}$ | effective crystal growth rate |
| $V_m$ | crystal molar volume |
| Vit1 | bulk metallic glass of composition $Zr_{41.2}Ti_{13.8}Cu_{12.5}Ni_{10}Be_{22.5}$ |

## Acknowledgments

We are thankful to Prof. Dr. Eduardo B. Ferreira of EESC-USP, Brazil for bringing the GRP method to our attention and for his critical review of this manuscript, and to the Brazilian agencies FAPESP (thematic project 07/08179-9) and CNPq for funding this research.

## References

[1] D. Xu, B.D. Wirth, J. Schroers, W.L. Johnson, Appl. Phys. Lett. 97 (2010) 024102-1.
[2] D. Turnbull, Contemp. Phys. 10 (1969) 473.
[3] A. Mashur, T.A. Waniuk, R. Busch, W.L. Johnson, Phys. Rev. Lett. 82 (1999) 2290.
[4] C.S. Ray, S.T. Reis, R.K. Brow, W. Höland, V. Rheinberger, J. Non-Cryst. Solids 351 (2005) 1350.
[5] D. Edwards, in: J.-C. Zhao (Ed.), Methods for Phase Diagram Determination, Elsevier BV, Oxford, 2007, pp. 341–360.
[6] E.S. Park, D.H. Kim, Appl. Phys. Lett. 86 (2005) 201912.
[7] K. Mondal, B.S. Murty, J. Non-Cryst. Solids 351 (2005) 1366.
[8] Z.P. Lu, H. Bei, C.T. Liu, Intermetallics 15 (2007) 618.
[9] W.J. Botta, F.S. Pereira, C. Bolfarini, C.S. Kiminami, M.F. de Oliveira, Philos. Mag. Lett. 88 (2008) 785.
[10] K.A. Jackson, D.R. Uhlmann, J.D. Hunt, J. Cryst. Growth 1 (1967) 1.
[11] M.L.F. Nascimento, L.A. Souza, E.B. Ferreira, E.D. Zanotto, J. Non-Cryst. Solids 351 (2005) 3296–3308.
[12] D.R. Uhlmann, H. Yinnon, C.-Y. Fang, Proc. 12th Lunar and Plan. Sci. Conf., 281, 1982.
[13] A.A. Cabral, C. Fredericci, E.D. Zanotto, J. Non-Cryst. Solids 219 (1997) 182–186.
[14] E.B. Ferreira, E.D. Zanotto, S. Feller, G. Lodden, J. Banerjee, E. Trent, M. Affatigato, J. Am. Ceram. Soc. 94 (2011) 3833.
[15] H.-J. Fecht, W.L. Johnson, Mater. Sci. Eng., A 375–377 (2004) 2–8.
[16] L. Battezzati, A. Castellero, P. Rizzi, J. Non-Cryst. Solids 353 (2007) 3318–3326.
[17] M.L.F. Nascimento, Ph.D Thesis, Universidade Federal de São Carlos, Brazil, 2004.
[18] G. Wilde, Thermochim. Acta 522 (2011) 20.
[19] B.A. Legg, J. Schroers, R. Busch, Acta Mater. 55 (2007) 1109.
[20] J. Gallino, M.B. Shah, R. Busch, Acta Mater. 55 (2007) 1367.
[21] G.J. Fan, J.F. Löffler, R.K. Wunderlich, H.-J. Fecht, Acta Mater. 52 (2004) 667.
[22] J.F. Löffler, Intermet. 11 (2003) 529.
[23] W.H. Wang, C. Dong, C.H. Shek, Mater. Sci. Eng. R. 44 (2004) 45.
[24] M. Imafuku, K. Saito, K. Kanehashi, S. Sato, A. Inoue, J. Non-Cryst. Solids 351 (2005) 3587–3592.
[25] C. Li, J. Saida, M. Matsushida, A. Inoue, Mater. Lett. 44 (2000) 80–86.
[26] C. Chen, M. Ferry, Trans. Nonferrous Met. Soc. China 16 (2006) 833–837.
[27] W.H. Wang, E. Wu, R.J. Wang, S.J. Kennedy, A.J. Studer, Phys. Rev. B 66 (2002) 104205.
[28] X. Wu, L. Meng, W. Zhao, Z. Suo, Y. Si, K. Qiu, J. Rare Earths 25 (2007) 189.
[29] G. Wang, J. Shen, J.F. Sun, B.D. Zhou, J.D. Fitz Gerald, D.J. Llewellyn, Z.H. Stachurski, Scr. Mater. 53 (2005) 641.
[30] E. Muller, K. Heide, E.D. Zanotto, J. Non-Cryst. Solids 155 (1993) 56.
[31] V.M. Fokin, E.D. Zanotto, J.W.P. Schmelzer, J. Non-Cryst. Solids 321 (2003) 52–65.
[32] V.M. Fokin, N.S. Yuritsyn, E.D. Zanotto, in: J.W.P. Schmelzer (Ed.), Nucleation Theory and Applications, Wiley-VCH Verlag GmbH, Weinheim, 2005, pp. 74–125.
[33] J. Paillier, A. Gebert, Thermochim. Acta 497 (2010) 85.
[34] Y. Birol, Mater. Sci. Eng. A249 (1998) 79.
[35] A. Gupta, S. Habibi, Mater. Sci. Eng. A133 (1991) 375.
[36] A. Calka, A.P. Randliński, Acta Metall. 35 (1987) 1823.
[37] T. Guo, M.L. denBoer, J. Non-Cryst. Solids 110 (1989) 111.
[38] U. Köster, Mater. Sci. Eng. 97 (1988) 233.
[39] A.A. Cabral, V.M. Fokin, E.D. Zanotto, J. Am. Ceram. Soc. 93 (2010) 2438–2440.
[40] V.M. Fokin, A.A. Cabral, R.M.C.V. Reis, M.L.F. Nascimento, E.D. Zanotto, J. Non-Cryst. Solids 356 (2010) 358–367.
[41] R. Müller, E.D. Zanotto, V.M. Fokin, J. Non-Cryst. Solids 274 (2000) 208–231.
[42] V.M. Fokin, E.D. Zanotto, N.S. Yuritsyn, J.W.P. Schmelzer, J. Non-Cryst. Solids 352 (2006) 2681–2714.
[43] J.W.P. Schmelzer, O.V. Potapov, V.M. Fokin, R. Müller, S. Reinsch, J. Non-Cryst. Solids 333 (2004) 150.
[44] J.W.P. Schmelzer, R. Müller, J. Möller, I.S. Gutzow, J. Non-Cryst. Solids 315 (2003) 144.
[45] M.L.F. Nascimento, E.D. Zanotto, J. Chem. Phys. 133 (174701) (2010) 1–10.
[46] M.L.F. Nascimento, V.M. Fokin, E.D. Zanotto, A.S. Abyzov, J. Chem. Phys. 135 (2011) 1.
[47] A.A. Cabral, V.M. Fokin, E.D. Zanotto, C.R. Chinaglia, J. Non-Cryst. Solids 330 (2003) 174.
[48] J.C. Mauro, Y. Yue, A.J. Ellison, P.K. Gupta, D.C. Allan, Proc. Natl. Acad. Sci. U. S. A. 106 (2009) 19780–19784.
[49] I. Gutzow, Contemp. Phys. 21 (1980) (p. 121 (I), p. 243 (II)).
[50] V.M. Fokin, A.M. Kalinina, V.N. Filipovich, J. Cryst. Growth 52 (1981) 115.
[51] V.M. Fokin, Ph.D Thesis, Silicate Chemistry Institute, Russia, 1980.
[52] J. Deubener, R. Brückner, M. Sternitzke, J. Non-Cryst. Solids 163 (1999) 1.
[53] J.J. Tuzzeo, Ph.D Thesis, Ohio State University, USA, 1976.
[54] M.F. Barker, T.-H. Wang, P.F. James, Phys. Chem. Glasses 29 (1988) 240.
[55] P.F. James, Phys. Chem. Glasses 15 (1974) 95.
[56] E.D. Zanotto, Ph.D Thesis, University of Sheffield, UK, 1982.
[57] L.L. Burgner, M.C. Weinberg, J. Non-Cryst. Solids 279 (2001) 28.
[58] V.M. Fokin, N.S. Yuritsin, O.V. Potapov, B.A. Shakhmatkin, N.M. Vedisheva, V.L. Ugolkov, A.G. Cherepova, J. Phys. Chem. 77N (10) (2003) 146.
[59] C.J.R. Gonzales-Olivier, P.S. Johnson, P.F. James, J. Mater. Sci. 14 (1979) 1159.
[60] K. Matusita, M. Tashiro, J. Non-Cryst. Solids 11 (1973) 471.
[61] E.D. Zanotto, M.L.G. Leite, J. Non-Cryst. Solids 202 (1996) 145.
[62] A.A. Cabral, V.M. Fokin, E.D. Zanotto, J. Non-Cryst. Solids 343 (2004) 85.
[63] R. Kelding apud M.L.F. Nascimento, Ph.D Thesis, Universidade Federal de São Carlos, Brazil, 2004.
[64] J.F. Löffler, J. Schroers, W.L. Johnson, Appl. Phys. Lett. 77 (2000) 681.
[65] S. Ding, J. Kong, J. Schroers, J. Appl. Phys. 110 (043508) (2011) 1–6.